Int. J. Heat Mass Transfer. Vol. 33, No. 8, pp. 1605–1617, 1990
Printed in Great Britain

0017-9310/90 $3.00 + 0.00

Double-diffusive convection in a rectangle with cooperating horizontal gradients of temperature and concentration

JAE MIN HYUN† and JIN WOOK LEE

Department of Mechanical Engineering, Korea Advanced Institute of Science and Technology, P.O. Box 150, Chong Ryang, Seoul, Korea

(*Received* 13 *June* 1989)

Abstract—Numerical results are presented of double-diffusive convection in a rectangular cavity. The externally imposed temperature and concentration gradients are antiparallel and aligned in the horizontal direction, constituting the cooperating gradients flow configuration. As a sequel to the previous account on the opposing gradients situation, the present paper provides comprehensive numerical solutions to the full, time-dependent Navier–Stokes equations at large thermal (R_t) and solutal (R_s) Rayleigh numbers. The details of velocity, thermal and solutal structures are revealed for a large Lewis number. In an analogous manner to the cases of opposing gradients, four distinct steady-state flow regimes are identified as the buoyancy ratio R_ρ ($=R_s/R_t$) varies over a wide range. When R_ρ is moderate, the multi-layered flow structure in the interior core is discernible; the associated S-shaped thermal field and the step-like concentration field are clearly disclosed. Time-evolutions of the flow developments are displayed. The major discrepancies between the results of the cooperating gradient cases and the opposing gradient cases are exposed. The present numerical results are found to be qualitatively consistent with the available experimental observations. Based on the numerical data, the steady-state mean Nusselt number $\overline{Nu}$ and the Sherwood number $\overline{Sh}$ are computed over a broad range of R_ρ. Differences are noted in the behavior of $\overline{Nu}$ and $\overline{Sh}$ with varying R_ρ between cooperating gradient flows and opposing gradient flows.

1. INTRODUCTION

LEE AND HYUN [1] presented a detailed numerical account of double-diffusive convection in a rectangular cavity. The numerical studies were obtained by solving the complete, time-dependent Navier–Stokes equations at large thermal (R_t) and solutal (R_s) Rayleigh numbers. The motion was initiated by the externally imposed gradients of the two diffusive properties, i.e. heat and solute, both of which were applied in the horizontal direction. The significance of such horizontally-aligned gradients of the diffusive properties has been stressed previously (see, e.g. Ostrach [2]). In particular, as was observed by Kamotani *et al.* [3], Wang *et al.* [4] and Lee *et al.* [5], this flow configuration is of relevance to industrial applications in modern material processing, among others. Some of the salient flow characteristics of this fluid system have been explored by the experimental endeavors cited in the above. One notable accomplishment has been a conclusive demonstration of the existence of the layered flow structure, together with the attendant characteristic thermal and solutal distributions, in the interior core of the cavity. The experimental flow visualizations by Lee *et al.* [5] confirmed that the layered structure was established under pertinent parameter settings.

In order to complement and reinforce the prior experimental investigations, comprehensive numerical simulations have been performed by the present authors. Obviously, since the Lewis number Le is large, the solutal boundary layer becomes extremely thin; resolving this thin layer has been a major obstacle hampering tangible progress in numerical studies of double-diffusive phenomena. By utilizing the much expanded computing resources of the current computer facilities, we were able to obtain numerical solutions to the full Navier–Stokes equations [1]. As a sequel to that work, the present paper will continue to report on the extensive numerical results.

In ref. [1], the horizontal gradients of temperature and concentration of a heavier substance were aligned parallel to each other. Consequently, the buoyancy effects due to thermal and solutal gradients were counteracting, creating a flow configuration with so-called opposing gradients [2]. The numerical results, as well as the preceding experimental data, pertaining to the opposing case were analyzed in ref. [1].

In the present paper, the flow configuration with cooperating gradients will be dealt with. As shown in Fig. 1, for definiteness, the left vertical wall at $X = 0$ represents the low-temperature (θ_l) and high-concentration (C_h) boundary, and the right vertical wall at $X = 1$ denotes the high-temperature (θ_h) and low-concentration (C_l) boundary. As is intuitively clear, the buoyancies due to the thermal and solutal effects

† Author to whom all correspondence should be addressed.

NOMENCLATURE

Ar	aspect ratio, H/L
C_h	dimensional concentration at the high-concentration side wall
C_l	dimensional concentration at the low-concentration side wall
ΔC	concentration difference, $C_h - C_l$
D	mass diffusivity
g	gravity
H	height of cavity
L	width of cavity
Le	Lewis number, κ/D
Nu	local Nusselt number
$\overline{Nu}$	mean Nusselt number
Pr	Prandtl number, ν/κ
Ra	effective Rayleigh number, $R_s + Le^{1/2} R_t$
R_s	solutal Rayleigh number, $g\beta_s \Delta C L^3/\kappa\nu$
R_t	thermal Rayleigh number, $g\beta_t \Delta\theta L^3/\kappa\nu$
R_ρ	buoyancy ratio, $\beta_s \Delta C/\beta_t \Delta\theta$
S	nondimensional concentration
Sh	local Sherwood number
$\overline{Sh}$	mean Sherwood number
T	nondimensional temperature
U	nondimensionalized horizontal velocity component
u	dimensional horizontal velocity component
V	nondimensionalized vertical velocity component
v	dimensional vertical velocity component
X	nondimensional horizontal coordinate
x	dimensional horizontal coordinate
Y	nondimensional vertical coordinate
y	dimensional vertical coordinate.

Greek symbols

β_s	coefficient of volumetric expansion with concentration
β_t	coefficient of volumetric expansion with temperature
δ_s	solutal boundary layer thickness
δ_t	thermal boundary layer thickness
θ_h	dimensional temperature at the high-temperature side wall
θ_l	dimensional temperature at the low-temperature side wall
$\Delta\theta$	temperature difference, $\theta_h - \theta_l$
κ	thermal diffusivity
ν	kinematic viscosity
ρ	dimensional density
ρ^*	nondimensional density
ρ_0	dimensional reference density
τ	nondimensional time
τ_h	nondimensional heat-up time scale
τ_s	nondimensional 'e-folding time' for a purely solutal convection
ψ	nondimensional stream function.

are mutually augmenting; thus this is termed the cooperating case. The rectangular cavity is of width L and height H, and the Cartesian coordinates (x, y), with the corresponding velocity components (u, v), are denoted. Initially, the fluid is motionless, and the temperature and concentration are uniform throughout at $\theta_0 = (\theta_h + \theta_l)/2$ and $C_0 = (C_h + C_l)/2$, respectively. At the initial instant $t = 0$, the temperature and concentration at the vertical side walls are abruptly altered, and they are maintained thereafter.

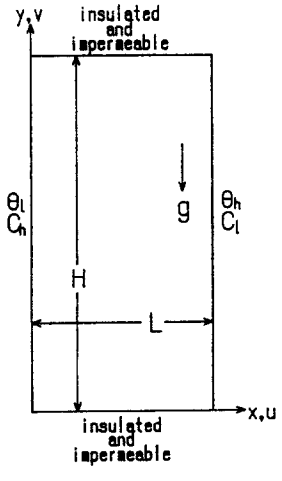

FIG. 1. Flow configuration and coordinate system.

The numerical methodologies and the subsequent analyses of the numerical data proceed in the same way as in ref. [1]. For the governing equations, the boundary and initial conditions, and the specific numerical model used, the reader is referred to ref. [1]. The values of the relevant parameters used in the study are identical to those in ref. [1], i.e. the Lewis number, $Le = 100$; the Prandtl number, $Pr = 7$; and the aspect ratio (H/L), $Ar = 2$, with the exception that the solutal Rayleigh number $R_s = 1.38 \times 10^8$ and the flow configuration is of a cooperating type instead of the opposing type of ref. [1]. In this paper, we shall only illuminate the essential results of numerical simulations and discuss the eminent characteristics of flow, thermal and solutal fields for the flows with cooperating horizontal gradients. Cross-checking of the present numerical results with the available experimental observations as well as the flows with opposing gradients will be conducted.

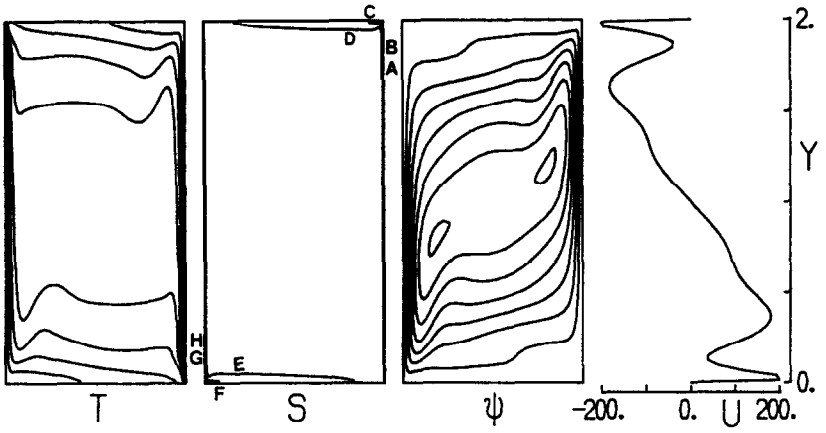

FIG. 2. Plots of isotherms, isohalines, stream functions and vertical profile of horizontal velocity at mid-width. Conditions are $R_\rho = 20$ and $\tau = 0.005$. Values for isotherms are, from left to right, -0.389, -0.278, -0.167, -0.0556, 0.0556, 0.167, 0.278 and 0.389. Values for isohalines are: (A) -0.389; (B) -0.278; (C) -0.167; (D) -0.0556; (E) 0.0556; (F) 0.167; (G) 0.278; (H) 0.389. Values for ψ are, from boundaries to interior, 15, 30, 45, 60, 75, 90 and 105.

2. RESULTS AND DISCUSSION

First, we shall describe the gross features of the early time flow characteristics. In the early phase well within the heat-up time scale τ_h [6], owing to the large difference in diffusivities of heat and concentration, the overall thermal and velocity fields resemble those of purely thermal convections. In the bulk of cavity the concentration is at the initial uniform value $S = 0.0$, except within the extremely thin solutal boundary layers adjacent to the vertical side walls. The above-stated general pattern is similar to that observed in the opposing gradient case [1]. However, one notable difference is seen with regard to the existence of the thin, localized corner regions of horizontally advancing fluids along the top and bottom boundaries [7]. Unlike the opposing case, such small regions of horizontally moving fluids are not visible in the present cooperating case, since the two buoyancy effects are augmenting each other. Figure 2 exemplifies the stream patterns at very small times.

We shall now look into the details of the flow fields as they are explicitly influenced by the relative magnitudes of the two buoyancy effects. When the buoyancy ratio R_ρ [$= R_s/R_t$] is sufficiently small, due to the dominance of the thermal buoyancy, the entire time-evolving processes are governed primarily by the thermal convection. Figure 3 provides exemplary results for a small buoyancy ratio ($R_\rho = 4.0$) at a large time ($\tau = 1.0$). As anticipated, the thermal and velocity fields are similar to those of pure thermal convection. As ascertained previously, since the thermal diffusivity is much greater than the solutal diffusivity, i.e. $Le = 100.0$, the thermally-driven flow field is established in much of the cavity at small times. Consequently, the mass diffusion into the core region is impeded by vigorous thermally-induced convective activities. Thus, solutal stratification takes place only in narrow strips very close to the top and bottom end walls. In the bulk of the cavity, the concentration is still at the initial uniform value $S = 0.0$. The vertical profile of the horizontal velocity component suggests boundary layer-type behavior in the regions very close to the horizontal end walls.

When the effects of thermal and solutal buoyancies are comparable, i.e. for intermediate values of R_ρ, complex, yet highly intriguing, flow characteristics are apparent. Figures 4–6 display the results when $R_\rho = 41.0$. At very early times, as remarked earlier, the general flow behavior is akin to that of pure thermal convection. As shown in Fig. 4(a) at $\tau = 0.05$, in the interior core, the thermal field is nearly linearly stratified, the concentration being at the uniform value ($S = 0.0$), and counter-clockwise circulation is seen. However, in the sizeable portions of the cavity near the top and bottom horizontal walls, the solutal field displays a near-linear stratification, and the velocities are reduced in strength. As time progresses, the regions near the top and bottom end walls in which the solutal field is stratified expand toward the mid-height. The beginning of the formation of layered flow structure is discernible (see Fig. 4(b) at $\tau = 0.5$). Notice that almost stagnant regions exist near the horizontal walls. The layered flow structure in the interior core becomes more distinct as time elapses further (see Fig. 4(c) at $\tau = 0.7$). In the regions adjacent to the top and bottom horizontal walls, the velocities are very small and these areas themselves have decreased in size. At this time instant, three layers have been fully established and two more layers begin to form. The time-evolving pictures of Fig. 4 show that the top and bottom regions of constant temperatures shrink in size as thermal convection intensifies in these regions as time progresses. The magnitudes of the velocities in the core tend to be smaller than the values of purely thermal convection at the same thermal

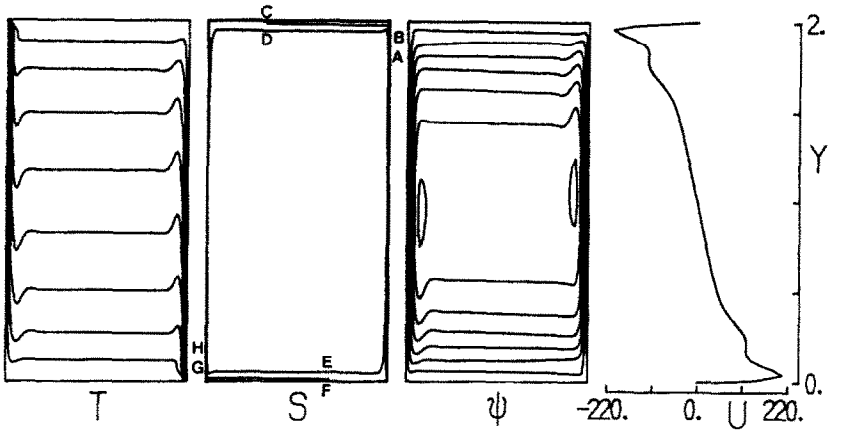

FIG. 3. Plots of isotherms, isohalines, stream functions and vertical profile of horizontal velocity at mid-width. Conditions are $R_\rho = 4.0$ and $\tau = 1.0$. Values for isotherms and isohalines are the same as in Fig. 2. Values for ψ are 10, 20, 30, 40, 50, 60 and 70.

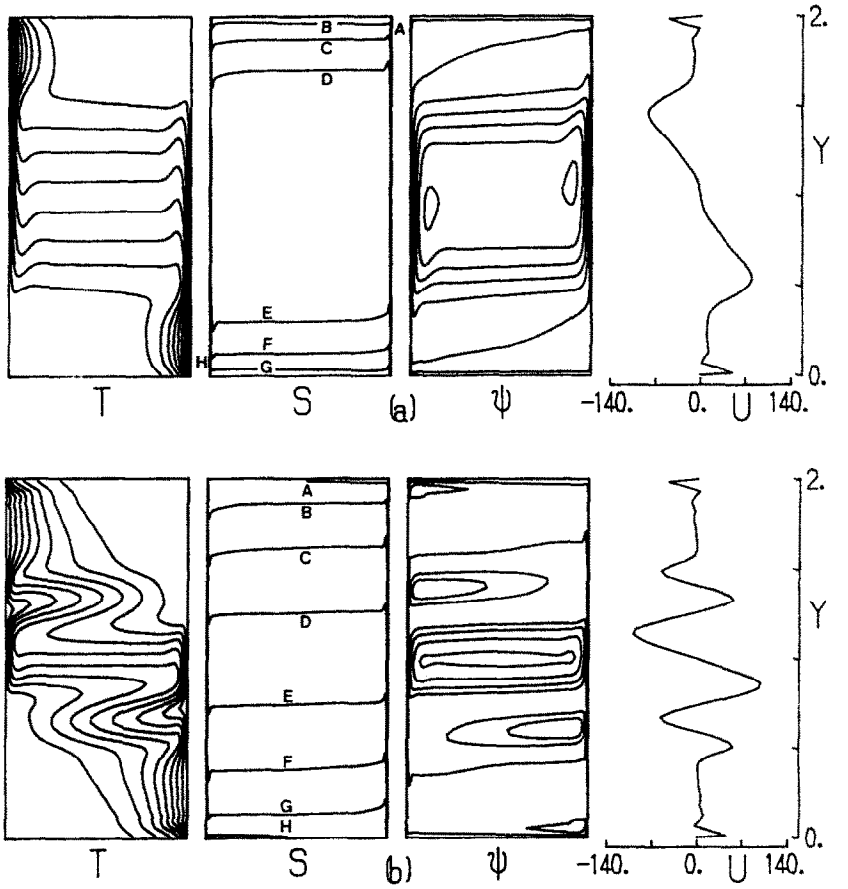

FIG. 4. Time evolving plots of isotherms, isohalines, stream functions and vertical profile of horizontal velocity at mid-width for $R_\rho = 41$. Times are $\tau = 0.05$ (a), 0.5 (b), 0.7 (c) and 1.0 (d). Values for isotherms and isohalines are the same as in Fig. 2. Values for ψ are: (a) 1, 3, 8, 14, 20, 26 and 32; (b) 1, 2, 3, 6, 9, 13.5 and 18; (c) 1, 2, 4, 5, 7 and 11; (d) 1, 1.7, 5, 10, 15 and 19.

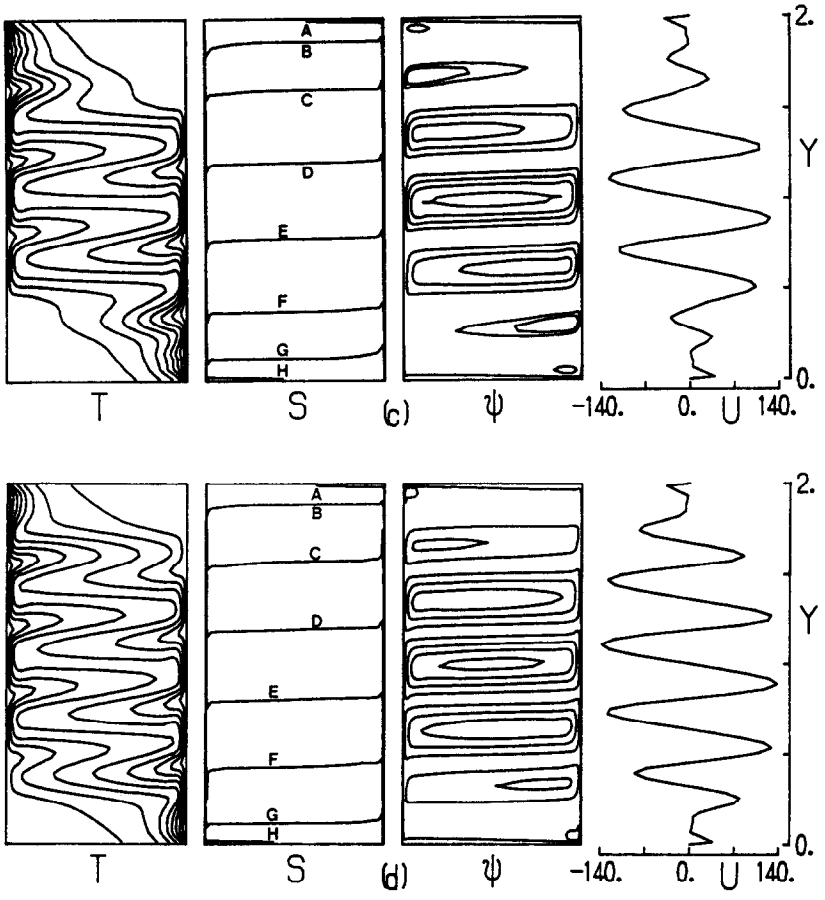

FIG. 4.—*Continued*

Rayleigh number (see the results of pure thermal convection of, e.g. ref. [8]). This is attributable to the presence of the stably-stratified solutal field, which inhibits the thermal convective activity in the interior. At large times (see Fig. 4(d) at $\tau = 1.0$), five layers have been fully developed; it can be ascertained that the entire cavity has been divided into five mini-cavities. The velocity and thermal fields within each layer resemble those of pure thermal convection in a shallow cavity with a correspondingly low thermal Rayleigh number. Small pockets of isothermal regions are visible near the top right and bottom left corners.

Figure 5 illustrates the large-time vertical profiles of the major flow properties for the results displayed in Fig. 4. The temperature and concentration profiles are along the mid-width $X = 0.5$, and the local Nusselt (Nu) and Sherwood (Sh) numbers at $X = 0$ are plotted for three time instants. The times are $\tau = 0.005$, typifying the flow well before the forming of the layered structure; $\tau = 0.6$, when three layers are established in the middle portions; and $\tau = 1.0$, when five layers are fully developed throughout the whole cavity. Much in line with the results of the opposing gradient case (see Fig. 6 of ref. [1]), the characteristic S-shaped temperature profile and the step-like concentration distribution are clearly depicted. The profile of the local Nusselt number possesses three local maxima at $\tau = 0.6$ and five local maxima at $\tau = 1.0$. These are strongly suggestive of the significant influence that the interior flow pattern exerts on the heat transfer near the side wall. It should also be pointed out that Nu is nearly zero very close to the bottom wall. This is in accord with the existence of the isothermal pockets near the bottom left corner area (see Fig. 4). As observed for the opposing gradient case (see Fig. 6 of ref. [1]), Sh is insensitive to the precise flow structure in the interior; the local mass transfer is principally governed by the very thin solutal boundary layer structure, and the flow within this layer is little influenced by the overall flows in the core.

In an effort to scrutinize further the details of the boundary layers, the horizontal profiles along the mid-height ($Y = Ar/2.0$) at $\tau = 1.0$ of the principal flow variables are exhibited in Fig. 6. The ratio of the thickness of the thermal and solutal boundary layers, (δ_t/δ_s), has been estimated as $O(LeR_\rho)^{1/4}$ by Wang *et al.* [4]. Examination of the numerical data of Fig. 6 points to the consistency with this scaling. The results of the run shown in Figs. 4–6 can be compared with the experimental measurements of Lee *et al.* [5]. The

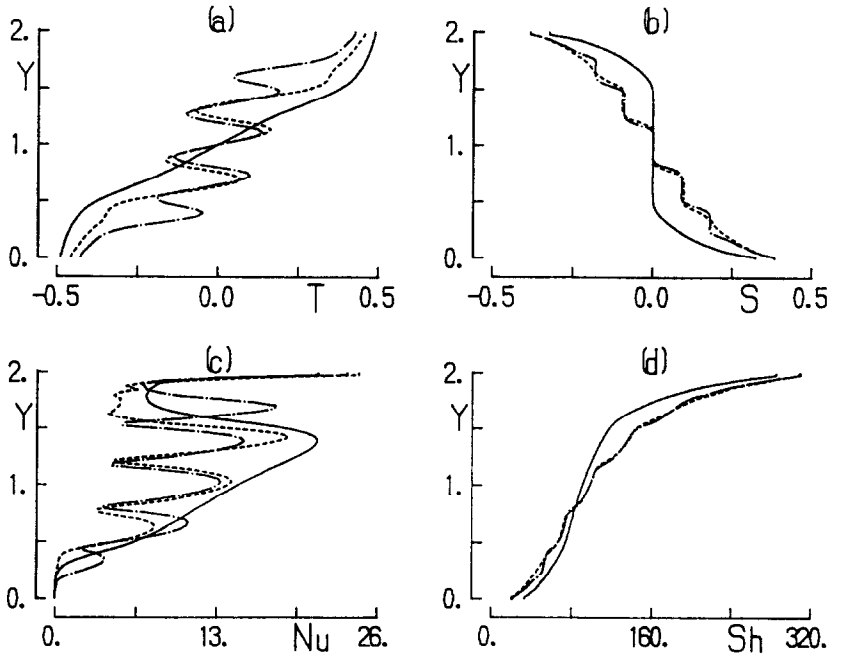

FIG. 5. Vertical profiles of (a) temperature and (b) concentration at $X = 0.5$. (c) Local Nu and (d) Sh at $X = 0$. Condition is: $R_\rho = 41$. Times are: ——, $\tau = 0.05$; – – –, $\tau = 0.6$; — · — · —, $\tau = 1.0$.

numerical computations were performed by using the same values of the parameters as those of the experiments of ref. [5]. The large-time behavior of the numerical results shows substantial agreement with the data of ref. [5].

Figure 7 demonstrates the effect of R_ρ on the fine details of the large-time flow characteristics; the value of R_ρ is still within the intermediate range such that the distinct layered flow structure in the interior is tenable. Figure 7(a) for $R_\rho = 20.0$ exemplifies the results when R_ρ is closer to the lower end of this intermediate range of R_ρ for the layered flow regime. The gross flow properties are similar to those already presented in Fig. 4(d) for $R_\rho = 41.0$. However, the thermal buoyancy is comparatively stronger for the case of $R_\rho = 20.0$ than for $R_\rho = 41.0$; the localized isothermal zones surrounding the top right and bottom left corners are smaller in size in Fig. 7(a) than in Fig. 4(d), indicating more vigorous thermally-induced activities in the bulk of the core. In the solutal field, Fig. 7(a) shows that, compared to that of Fig. 4(d), the height of each layer in the core is larger, the thickness of the layer interface is smaller, and the step-change of the concentration across the interface is more abrupt. Also, the strengths of the horizontal velocity fluctuations in the interior layered regions tend to increase as R_ρ decreases within the intermediate range. Figure 7(b) at $R_\rho = 60.0$ exhibits the opposite trend as R_ρ increases toward the upper end of the intermediate range. The thermal buoyancy is now less vigorous; thus, only three distinct velocity layers are visible in the interior. The thermal buoyancy is not strong enough to overcome the effect due to the substantial concentration distribution in parts of the flow field near the top and bottom horizontal walls; the fluids in these regions are nearly stagnant, and these stagnant areas occupy greater portions of the cavity as R_ρ increases further. Also noticeable are the enlarged isothermal zones near the top right and bottom left corners.

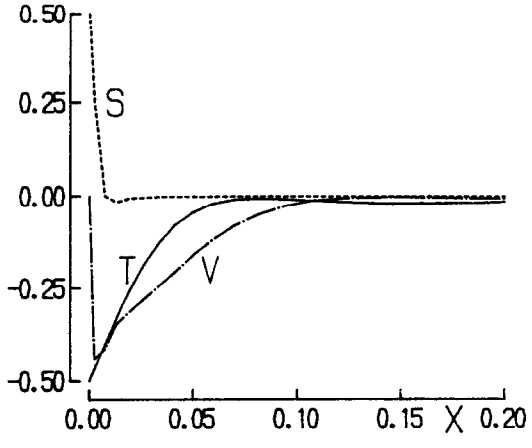

FIG. 6. Horizontal profiles of temperature (T), concentration (S) and vertical velocity ($V^* = V/1000$) at mid-height ($Y = Ar/2$). Conditions are $R_\rho = 41$ and $\tau = 1.0$.

We now turn to the question of the flow behavior when R_ρ takes a very large value. Figure 8 typifies the time-dependent qualitative flow character under an extreme R_ρ ($R_\rho = 3000.0$). At very small times, as asserted previously, the thermal buoyancy is still dominant regardless of R_ρ; Fig. 8(a) at $\tau = 0.05$ is

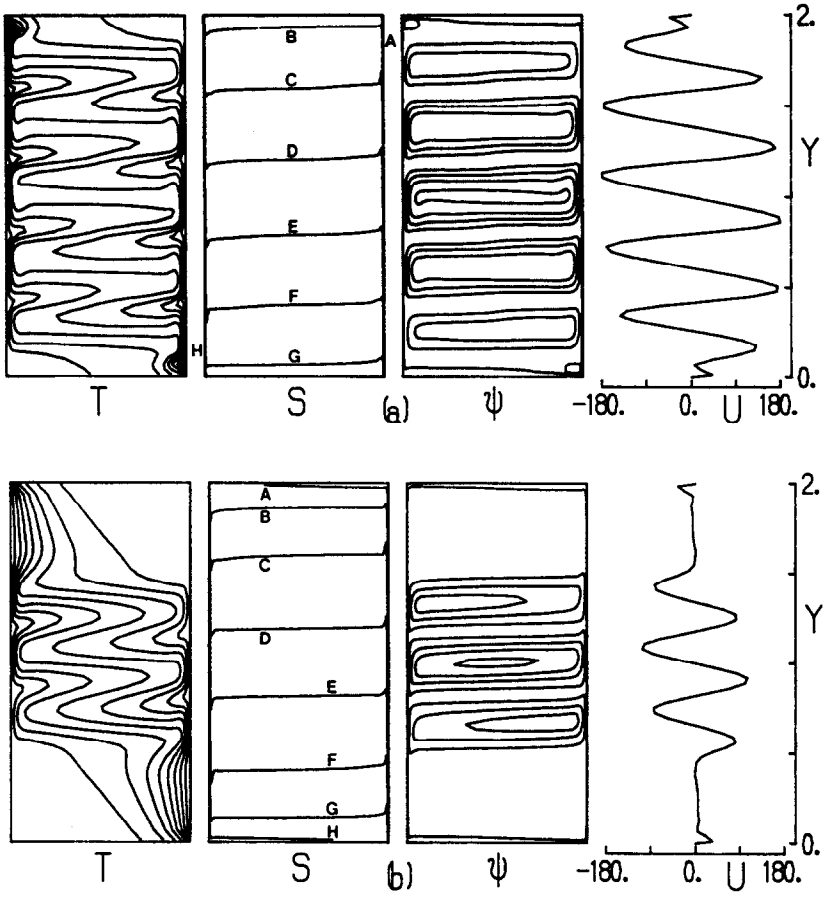

FIG. 7. Plots of isotherms, isohalines, stream functions and vertical profile of horizontal velocity at mid-width ($\tau = 1.0$). Buoyancy ratios are $R_\rho = 20$ (a) and 60 (b). Values for isotherms and isohalines are the same as in Fig. 2. Values for ψ are: (a) 1.5, 2.5, 8, 14, 20 and 26; (b) 1, 4.5, 8, 11.5 and 15.

qualitatively similar to Fig. 4(a). At a later time, however, the difference in flow characteristics becomes conspicuous. At moderate times (see Fig. 8(b) at $\tau = 0.3$), the temperature is weakly stratified in the vertical direction only in a narrow band near the mid-height. Corresponding to this thermal stratification, a weaker counter-clockwise circulation of restricted vertical extent is seen near the mid-height in the velocity field. In this region, the concentration is still at the initial uniform value $S = 0.0$. At a still later time leading to the steady-state (see Fig. 8(c) at $\tau = 1.0$), since the solutal buoyancy far outweighs the thermal buoyancy, the overall flow pattern resembles that of pure solutal convection. The concentration shows a near-linear stratification in the vertical direction; the temperature field is qualitatively akin to the conduction-controlled situations, and the overall velocity field in the bulk of the cavity is fairly quiescent.

Figure 9 is presented in order to delineate the changes in the character of the steady flow, ranging from the layered flow regime for intermediate values of R_ρ to the solutal-dominant regime for large values of R_ρ. As is evident in Fig. 9(a) for $R_\rho = 100.0$, a single thermally-driven counter-clockwise circulation, together with the vertical temperature stratification, is discernible in a narrow band surrounding the mid-height. As R_ρ increases (see Fig. 9(b) for $R_\rho = 500.0$), this thermally-induced circulation weakens in magnitude and shrinks in size. At a still further increase of R_ρ (see Fig. 9(c) for $R_\rho = 1000.0$), the bulk of the interior is, by and large, motionless; only the weak horizontal velocities in thin strips adjacent to the horizontal boundaries are seen. The thermally-induced motions in the interior core are impeded by the well-established stably-stratified solutal field. It is also apparent that the thermal field in the bulk of the cavity becomes conduction-dominant when R_ρ takes a sufficiently large value.

In summary, four distinct flow regimes have been identified as R_ρ varies, in a manner similar to the case of opposing gradient configurations. They are: (1) the thermal effect-dominant regime; (2) the regime in which both the thermal and solutal effects are comparable, producing the well-defined layered flow structure in the interior core; (3) the regime in which the solutal effect is prominent in the bulk of the cavity,

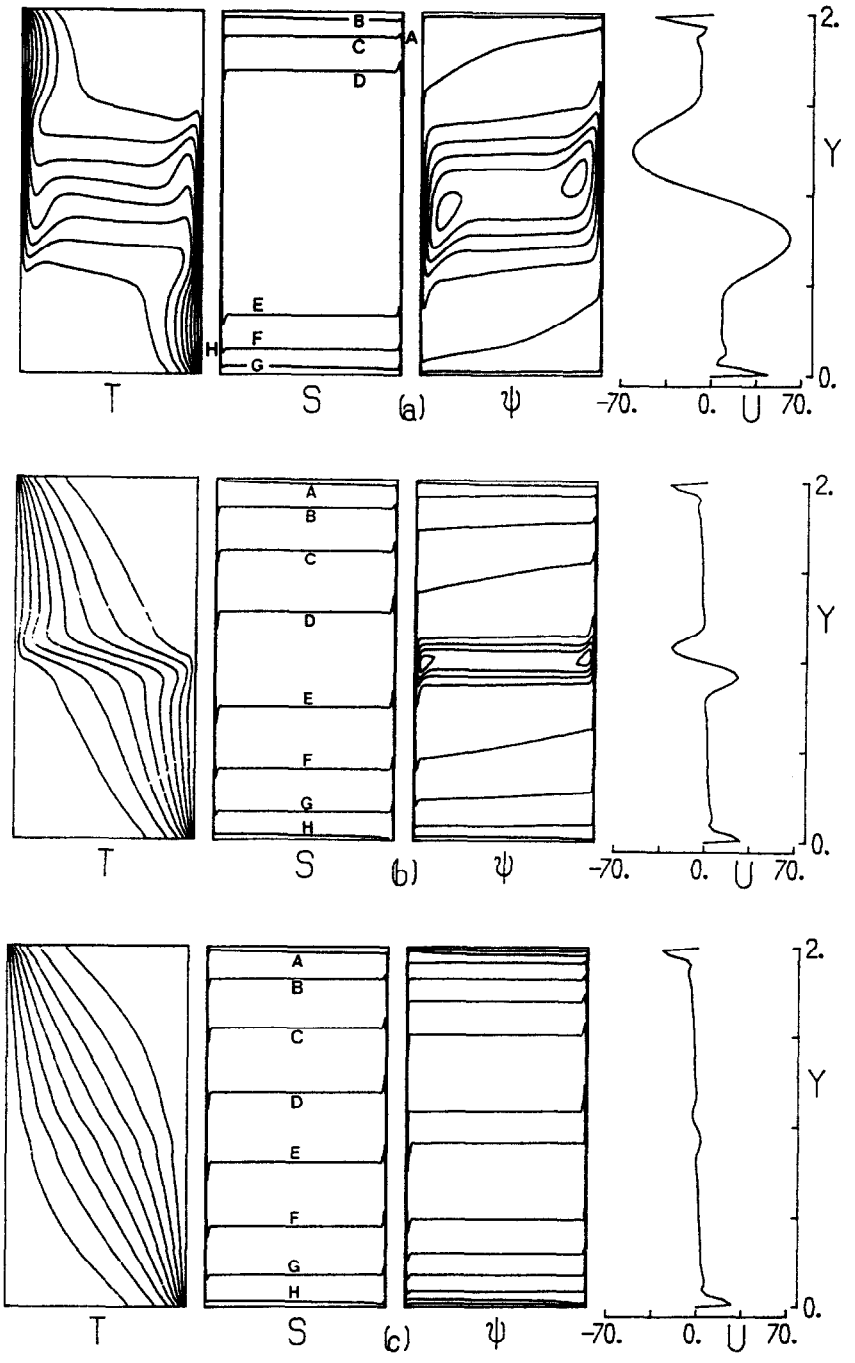

FIG. 8. Time evolving plots of isotherms, isohalines, stream functions and vertical profile of horizontal velocity at mid-width for $R_\rho = 1000$. Times are $\tau = 0.05$ (a), 0.3 (b) and 1.0 (c). Values for isotherms and isohalines are the same as in Fig. 2. Values for ψ are: (a) 1, 3, 8, 13, 18, 23 and 28; (b) 0.7, 1.6, 2.5, 3.4, 4.3, 5.2, 6.1 and 7.0; (c) 0.54, 1.08, 1.62, 2.16, 2.70, 3.24 and 3.78.

with the exception of the thin core band near the mid-height where the thermal effect is still appreciable; (4) the solutal effect-dominant regime. Based on flow visualization studies, Lee *et al.* [5] proposed three flow regimes, which correspond to regimes (1), (2) and (4) described above. The comparisons of the flow data obtainable by the present numerical results and the experimental visualizations of ref. [5] exhibit generally satisfactory agreement. The agreement is good both in the global qualitative characterizations and in the specific profiles of the essential physical variables. It is perhaps worth pointing out that the regime categorized in

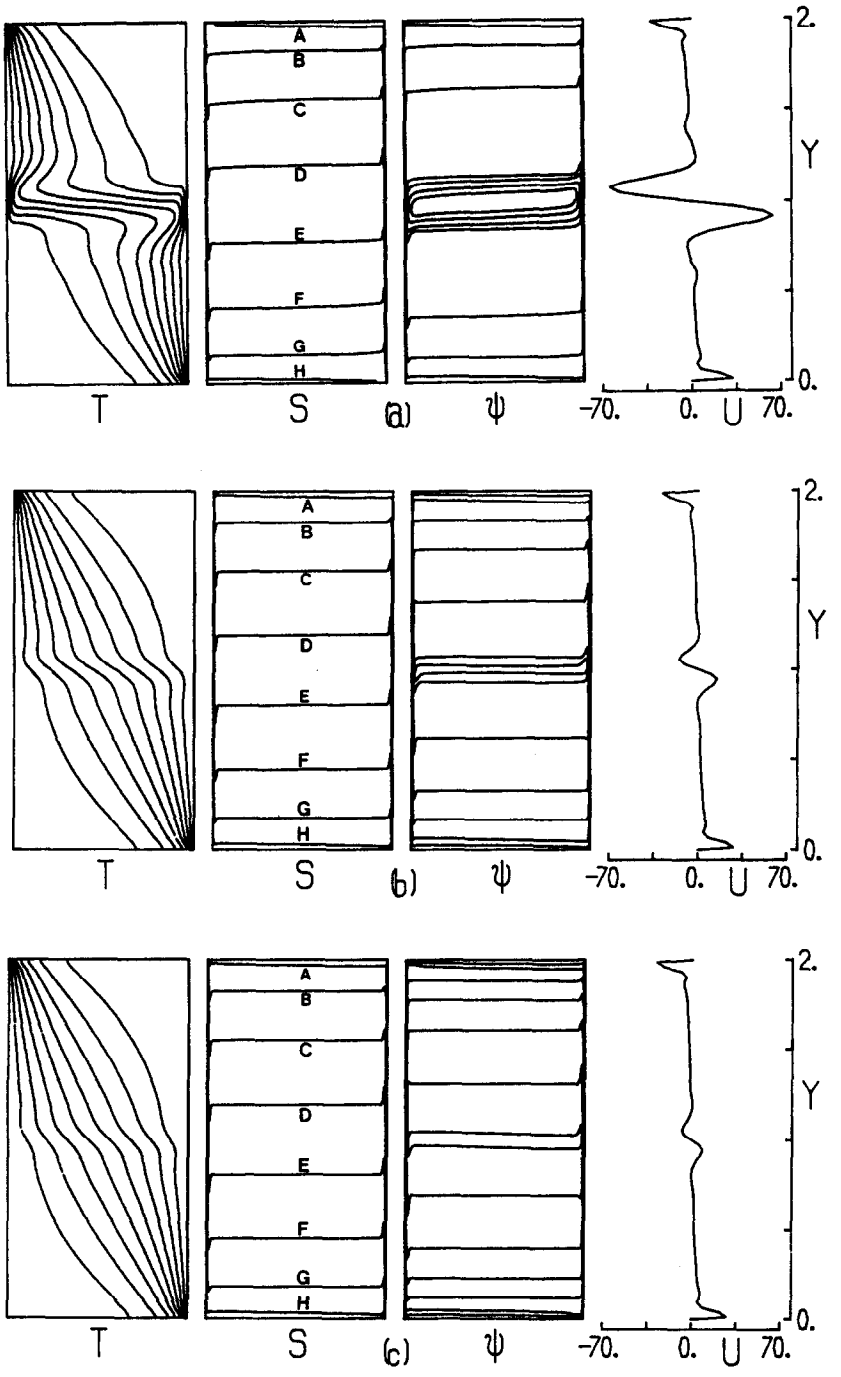

FIG. 9. Plots of isotherms, isohalines, stream functions and vertical profile of horizontal velocity at mid-width ($\tau = 1.0$). Buoyancy ratios are $R_\rho = 100$ (a), 500 (b) and 1000 (c). Values for isotherms and isohalines are the same as in Fig. 2. Values for ψ are: (a) 1, 2, 3, 4, 5, 7 and 9; (b) 0.7, 1.4, 2.1, 2.8, 3.5, 4.2 and 4.9; (c) 0.6, 1.2, 1.8, 2.4, 3, 3.6 and 4.2.

the above as (3) was not classified explicitly in the experimental investigations by Lee *et al.* [5]. Regime (3) is located on the border line of the parameter space, and it could well be characterized as a subset to the generalized layered flow regime denoted as (2) in the above.

In order to portray the fine details of the steady-state behavior near the vertical walls, enlarged views of the horizontal profiles are depicted in Fig. 10. When the buoyancy ratio is large, the temperature variation in the close proximity of the wall becomes more rapid. The concentration profiles tend to be quite insensitive

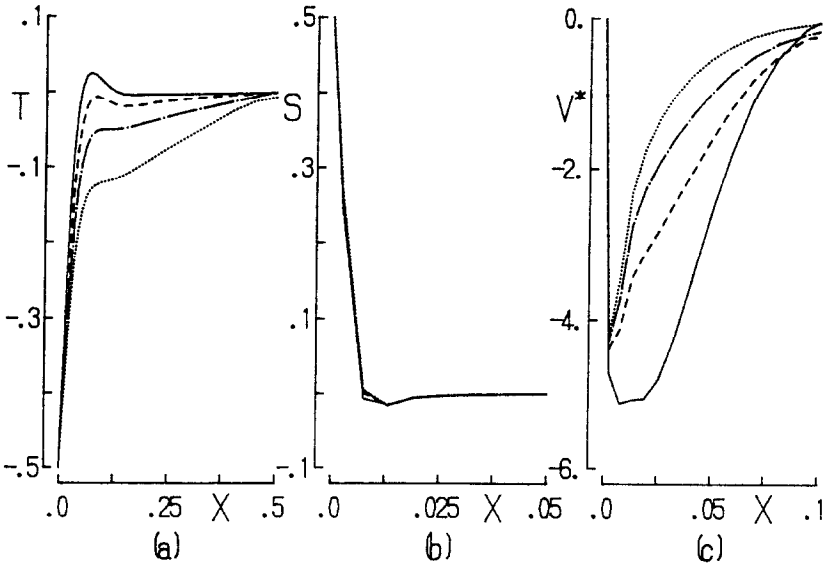

FIG. 10. Horizontal profiles of (a) temperature (T), (b) concentration (S), and (c) vertical velocity ($V^* = V/100$) near the low-temperature and high-concentration wall at $\tau = 1.0$. The values of R_ρ are: ——, $R_\rho = 20$; – – – –, $R_\rho = 41$; — · — · —, $R_\rho = 60$; · · · · · · · · ·, $R_\rho = 100$.

to the change in R_ρ. At a large Lewis number, the precise details of the solutal boundary layer structure are little affected by the interior flows. The vertical velocity profiles are suggestive of the typical boundary-type shapes. However, it is noticed that, in contrast to the opposing gradient cases (see Fig. 9 of ref. [1]), the maximum value of the magnitude of the vertical velocity decreases as R_ρ increases. At a small R_ρ, the augmentation of the buoyancies is quite effective under the overriding influence of the dominant thermally-induced effect. On the other hand, at a large R_ρ, as ascertained previously, the thermally-driven convection occupies a smaller portion near the mid-height of the cavity, confined to a mini-cavity. This implies that the global augmentation of the buoyancies in the entire cavity is less complete at a large R_ρ.

The specific impact of R_ρ on the resulting steady-state density profile is illustrated in Fig. 11, where the nondimensionalized density ρ^* is defined as

$$\rho^* = \frac{1}{\beta_s \Delta C}\left(\frac{\rho}{\rho_0} - 1\right) = -\frac{T}{R_\rho} + S.$$

The general behavior of ρ^* as R_ρ increases is similar to that of the opposing gradient cases (see Fig. 10 of ref. [1]), i.e. smooth variations at low R_ρ, step-like distributions at moderate R_ρ, and again smooth profiles at large R_ρ. Comparisons of the two cases reveal the nonexistence of the patches of localized gravitationally unstable configuration in the present results. This can be explained by arguing that, under the cooperating gradients, the buoyancies are augmenting; thus, even very near the horizontal boundaries, the overall density is stably stratified in the vertical direction.

As was previously done for the opposing gradient cases (see Table 1 of ref. [1]), the heat and mass transfer rates across the cavity are computed by utilizing the numerical results. Table 1 lists the mean Nusselt number

$$\overline{Nu} = \frac{1}{Ar}\int_0^{Ar} (\partial T/\partial X)_{X=0}\, \mathrm{d}Y$$

and the mean Sherwood number

$$\overline{Sh} = \frac{1}{Ar}\int_0^{Ar} -(\partial S/\partial X)_{X=0}\, \mathrm{d}Y$$

evaluated at $\tau = 1.0$. It should be remarked that this time instant corresponds to four e-folding time scales

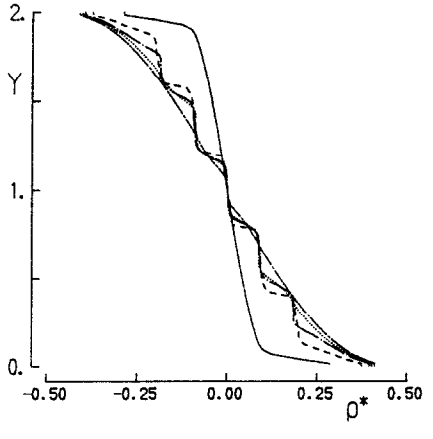

FIG. 11. Nondimensional density ρ^* at $X = 0.5$ at $\tau = 1.0$. The values of R_ρ are: ——, $R_\rho = 4$; – – – –, $R_\rho = 20$; — · — · —, $R_\rho = 41$; · · · · · · · · ·, $R_\rho = 60$; — · · — · · —, $R_\rho = 500$.

Table 1. Mean Sherwood $\overline{Sh}$ and Nusselt $\overline{Nu}$ numbers at a large time ($\tau = 1.0$)

R_ρ	$\overline{Sh}$	$\overline{Nu}$ DDC	$\overline{Nu}$ PTC
0.5	166.84	36.41	36.21
1.0	149.79	30.36	30.16
4.0	120.55	20.44	20.98
20.0	116.13	12.34	13.80
41.0	113.19	8.417	11.44
60.0	111.43	5.857	10.36
100.0	109.78	3.334	9.057
200.0	109.21	2.486	7.541
500.0	108.87	2.196	5.907
1000.0	108.72	2.134	4.897
3000.0	108.61	2.108	3.624
10000.0	108.59	2.104	2.610
PSC	108.58		

For the tabulation of $\overline{Nu}$, DDC denotes the case of double-diffusive convection, and PTC denotes the case of pure thermal convection. For the value of R_ρ, PSC indicates the case of pure solutal convection.

derivable for purely solutal convections [6]. At this time instant, the overall flows are substantially close to the steady-state when R_ρ is very large or small; when R_ρ is intermediate, very minor flow evolutions are seen in parts of the cavity; however, the temporal changes in the global flow patterns are insignificant. Consequently, the numerical data contained in Table 1 are representative of the steady-state or at least quasi-steady situations.

Inspection of Table 1 of the present paper and Table 1 of ref. [1] discloses that the heat transfer rates are, in general, greater for the cooperating cases than for the opposing cases. This is not surprising since the buoyant activities are more vigorous for the cooperating cases. Perusal of the data for $\overline{Nu}$ in Table 1 reveals that, when R_ρ is either very small or very large, the difference in $\overline{Nu}$ between the double-diffusive convection and the purely thermal convection is quite negligible. This can be easily explained by pointing out that these two extreme cases refer to the thermal effect-dominant or the solutal effect-dominant regimes. Consequently, the general heat transfer will be similar to that of single-diffusive convection. Obviously, the explicit nature of double-diffusive convection makes itself felt only when R_ρ is intermediate. In this regime, $\overline{Nu}$ for double-diffusive convection tends to be smaller than that for single-diffusive convection. The presence of the stably-stratified solutal field hinders the thermal convective activity, which is the principal mechanism of heat transfer, in much of the cavity.

Scrutiny of the mass transfer rates indicates that, when R_ρ exceeds some moderate values, $\overline{Sh}$ is nearly constant, approaching a value appropriate for the case of a purely solutal convection. $\overline{Sh}$ increases relatively steeply as R_ρ is reduced from moderate to very small values. An important aspect in the behavior of $\overline{Sh}$ is the existence of a minimum of $\overline{Sh}$ at a moderate value of R_ρ for the opposing cases (see Table 1 of ref. [1]). However, for the present cooperating cases, the two buoyancy effects are augmenting; consequently, the decrease of $\overline{Sh}$ with increasing R_ρ is monotonic. The above-cited patterns of the $\overline{Sh}$ variations with R_ρ are strong qualitative agreement with the experimental measurements of ref. [3]. Reference [3] proposed an empirical correlation, based on their experiments using a cavity of low aspect ratio, $\overline{Sh} = 0.67(Le\ Ra)^{1/4}$, where the effective Rayleigh number $Ra \equiv R_s + Le^{1/2} R_t$. Reference [3] further stated that this empirical formula would approach the relation tenable for a corresponding vertical flat plate when $Le\ Ra$ becomes very large. The values shown in Table 1 are slightly lower than these empirical predictions. As stressed earlier, these small quantitative differences could be traced to several experimental uncertainties and the unavoidable minor discrepancies stemming from the numerical simulation of such complex physical systems.

3. CONCLUSION

Numerical computations of the full, time-dependent Navier–Stokes equations have been conducted. For the flow configurations with horizontally-directed cooperating gradients of the diffusive properties, flow details have been acquired and analyzed.

At very small times, since $Le \gg 1$, the early time flow is akin to that of pure thermal convection. However, at intermediate and large times, explicit dependence of the flow on the buoyancy ratio R_ρ is conspicuous.

When R_ρ is sufficiently small, the entire temporal evolutions are governed primarily by the thermal buoyancy.

When R_ρ is moderate, the thermal and solutal buoyancies are comparable. The gross flow characteristics display substantial time-dependence. At moderate times, the solutal field is stratified in the regions near the top and bottom end walls, and these regions expand toward the mid-height. The layers form in the velocity field. At large times, the layered velocity field is established, together with the S-shaped temperature profiles and the step-like solutal profiles.The profile of the local Nusselt number possesses several maxima, but the local Sherwood number profile is insensitive to the precise flow structure in the interior. These eminent flow characteristics are in accord with the experimental visualizations of Lee *et al.* [5].

When R_ρ is very large, the global flow properties are similar to those of pure solutal convection. The bulk of the interior is largely motionless, and the thermal field is nearly conduction-dominant.

The flow regimes that can be categorized based on the numerical data are consistent with the experimental observations of Lee *et al.* [5].

The resulting overall density profile shows smooth variations at low R_ρ, step-like distributions at moderate R_ρ, and again smooth variations at large R_ρ.

Unlike the cases of opposing gradient configurations, the density is stably stratified throughout the entire cavity since the two buoyancies are augmenting.

When R_ρ is moderate, the mean Nusselt number $\overline{Nu}$ for double-diffusive convection tends to be smaller than that for single-diffusive convection, due to the presence of the stably-stratified solutal field. The mean Sherwood number $\overline{Sh}$ decreases monotonically as R_ρ increases. This is attributable to the fact that, in contrast to the opposing gradient case, the buoyancies are aiding in the present case. The qualitative behavior of $\overline{Nu}$ and $\overline{Sh}$ is consistent with the earlier experimental measurements [3].

Acknowledgements—The authors are grateful to the referee who provided detailed and constructive comments. This work was supported in part by a research grant from the Korea Science and Engineering Foundation (KOSEF).

REFERENCES

1. J. W. Lee and J. M. Hyun, Double-diffusive convection in a rectangle with opposing horizontal temperature and concentration gradients, *Int. J. Heat Mass Transfer* **33**, 1619–1632 (1990).
2. S. Ostrach, Natural convection with combined driving forces, *PhysicoChem. Hydrodyn.* **1**, 233–247 (1980).
3. Y. Kamotani, L. W. Wang, S. Ostrach and D. Jiang, Experimental study of natural convection in shallow enclosures with horizontal temperature and concentration gradients, *Int. J. Heat Mass Transfer* **28**, 165–173 (1985).
4. L. W. Wang, Y. Kamotani and S. Ostrach, Experimental study of natural convection in a shallow horizontal cavity with different end temperature and concentrations, Report FTAS/TR-82-164, Case Western Reserve University (1983).
5. J. Lee, M. T. Hyun and K. W. Kim, Natural convection in confined fluids with combined horizontal temperature and concentration gradients, *Int. J. Heat Mass Transfer* **31**, 1969–1977 (1988).
6. M. C. Jischke and R. T. Doty, Linearized buoyant motion in a closed container, *J. Fluid Mech.* **71**, 729–754 (1975).
7. S. Ostrach, D. Jiang and Y. Kamotani, Thermosolutal convection in shallow enclosures, *Proc. ASME–JSME Thermal Engng Joint Conf.*, Vol. 2, pp. 159–168 (1987).
8. J. M. Hyun and J. W. Lee, Numerical solutions for transient natural convection in a square cavity with different sidewall temperatures, *Int. J. Heat Fluid Flow* **10**, 146–151 (1989).

CONVECTION DOUBLEMENT DIFFUSIVE DANS UN RECTANGLE AVEC DES GRADIENTS HORIZONTAUX COOPERANTS DE TEMPERATURE ET DE CONCENTRATION

Résumé—Des résultats numériques sont présentés sur la convection doublement diffusive dans une cavité rectangulaire. Les différences de température et de concentration imposées extérieurement sont appliquées dans la direction horizontale et elles constituent la configuration de gradients coopérants pour l'écoulement. On donne des solutions numériques des équations complètes de Navier–Stokes pour des grands nombres de Rayleigh thermique (R_t) et solutal (R_s). Les détails des champs de vitesse, de température et de concentration sont révélés pour de grands nombres de Lewis. De façon analogue quatre régimes d'écoulement permanent sont identifiés quand le rapport R_ρ ($= R_s/R_t$) varie largement. Lorsque R_ρ est modéré, la structure de l'écoulement multicouche est discernable dans le coeur ; le champ thermique associé en S et le champ de concentration en escalier sont clairement disjoints. On expose les principales différences entre les résultats des cas à gradients coopérants et ceux à gradients opposés. Les résultats numériques sont qualitativement cohérents avec les observations expérimentales disponibles. Les nombres de Nusselt $\overline{Nu}$ et de $\overline{Sh}$ moyens en régime permanent sont calculés pour un large domaine de R_ρ. Les différences sont dégagées dans le comportement de $\overline{Nu}$ et $\overline{Sh}$, lorsque R_ρ varie, entre les écoulements à gradients coopérants et ceux à gradients opposés.

GLEICHGERICHTETE DOPPELT-DIFFUSIVE KONVEKTION IN EINEM RECHTECKIGEN HOHLRAUM MIT HORIZONTALEN GRADIENTEN

Zusammenfassung—In dieser Arbeit werden numerische Ergebnisse für die doppelt-diffusive Konvektion in einem rechteckigen Hohlraum vorgestellt. Die von außen aufgeprägten Temperatur- und Konzentrationsgradienten sind nicht-parallel und waagerecht ausgerichtet, wodurch eine gleichgerichtete Strömungssituation ensteht. In der Folge einer früher vorgestellten Arbeit über die gegengerichtete Strömungssituation werden hier numerische Lösungen der vollständigen zeitabhängigen Navier–Stokes-Gleichungen bei großen thermischen (R_t) und Konzentrations- (R_s) Rayleigh-Zahlen gezeigt. Es werden Geschwindigkeits-, Temperatur- und Konzentrationsfelder für eine große Lewis-Zahl vorgestellt. Ähnlich wie bei der gegengerichteten Situation ergeben sich vier Bereiche der stationären Strömung—abhängig vom Auftriebsverhältnis $R_\rho = (R_s/R_t)$. Bei mittleren Werten von R_ρ ist eine vielschichtige Strömungsstruktur im inneren Kern erkennbar; das damit verbundene S-förmige Temperaturfeld und das stufenförmige Konzentrationsfeld treten klar in Erscheinung. Es wird die zeitliche Entwicklung der Strömung vorgestellt. Ebenfalls werden die wesentlichen Unterschiede zwischen den Ergebnissen für den gleichgerichteten Fall gezeigt. Die numerischen Ergebnisse stimmen qualitativ mit verfügbaren Versuchsergebnissen überein. Auf der Grundlage der numerischen Daten werden für den stationären Fall mittlere Nusselt-Zahlen ($\overline{Nu}$) und Sherwood-Zahlen ($\overline{Sh}$) in einem weiten Bereich von R_ρ berechnet. Für beide Strömungssituationen werden die Unterschiede im Verhalten von $\overline{Nu}$ und $\overline{Sh}$ vorgeführt.

КОНВЕКТИВНЫЙ ТЕПЛО- И МАССООБМЕН В ПРЯМОУГОЛЬНОЙ ПОЛОСТИ ПРИ СОВМЕСТНО ДЕЙСТВУЮЩИХ ГОРИЗОНТАЛЬНЫХ ГРАДИЕНТАХ ТЕМПЕРАТУРЫ И КОНЦЕНТРАЦИИ

Аннотация—Представлены численные результаты по конвективному тепло- и массопереносу в прямоугольной полости. Приложенные извне градиенты температуры и концентрации являются антипараллельными и горизонтально направленными, определяя таким образом конфигурацию течения с однонаправленным подъемным действием градиентов. В продолжение предыдущего исследования случаев с противодействующими градиентами в данной статье приводятся численные решения полных нестационарных уравнений Навье–Стокса при больших значениях тепловых (R_t) и концентрационных (R_s) чисел Рэлея. Рассчитаны детали скоростных, температурных и концентрационных структур при больших значениях числа Льюиса. Как и в предыдущем исследовании, при варьировании отношения подъемных сил $R_\rho(=R_s/R_t)$ в широком диапазоне значений обнаружены четыре стационарных режима течения. При умеренных значениях числа R_ρ отчетливо проявляется многослойная структура течения во внутреннем ядре, а также ясно обнаруживаются S-образное тепловое поле и ступенчатое поле концентраций. Проиллюстрировано развитие течения во времени. Показаны основные расхождения между результатами для случаев с действующими в одном направлении и противодействующими градиентами. Показано, что полученные численные результаты качественно согласуются с имеющимися экспериментальными наблюдениями. На основе численных результатов рассчитаны стационарные средние значения чисел Нуссельта $\overline{Nu}$ и Шервуда $\overline{Sh}$ в широком диапазоне значений числа R_ρ. Отмечены различия в поведении чисел $\overline{Nu}$ и $\overline{Sh}$ с изменением значения числа R_ρ в случаях течения с действующими в одном направлении и противодействующими градиентами.